iScience

CellPress
OPEN ACCESS

Article

NRF3 upregulates gene expression in SREBP2-dependent mevalonate pathway with cholesterol uptake and lipogenesis inhibition

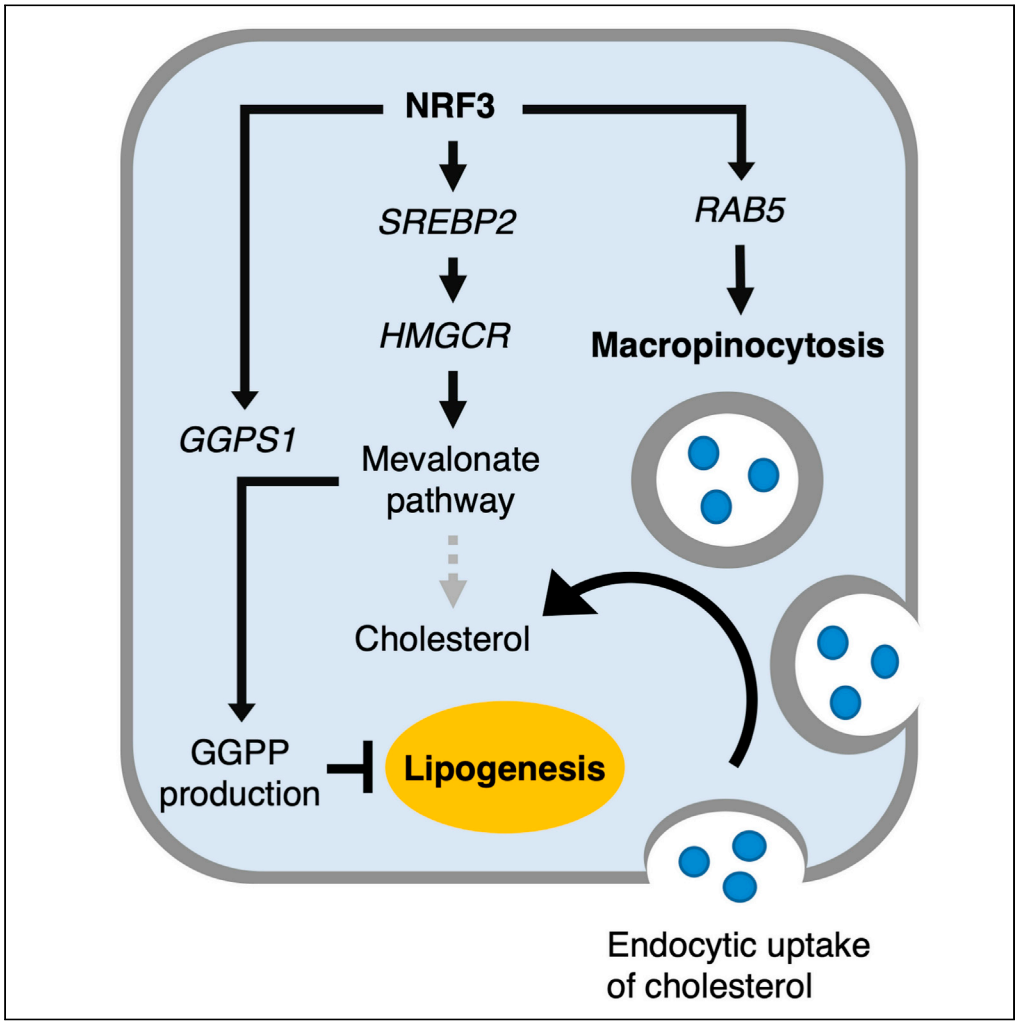

Tsuyoshi Waku, Toru Hagiwara, Natsuko Tamura, ..., Masayuki Yamamoto, Noriko Noguchi, Akira Kobayashi

akobayas@mail.doshisha.ac.jp

Highlights

NRF3 upregulates gene expression of enzymes in the mevalonate pathway

NRF3 induces *SREBP2* gene expression and interacts with active SREBP2 proteins

NRF3 reduces neutral lipid levels through GGPS1-mediated GGPP production

NRF3 enhances cholesterol uptake through RAB5-mediated macropinocytosis

Waku et al., iScience *24*, 103180
October 22, 2021
https://doi.org/10.1016/j.isci.2021.103180

iScience

CellPress
OPEN ACCESS

Article

NRF3 upregulates gene expression in SREBP2-dependent mevalonate pathway with cholesterol uptake and lipogenesis inhibition

Tsuyoshi Waku,[1] Toru Hagiwara,[2,6] Natsuko Tamura,[2,6] Yuri Atsumi,[2,6] Yasuomi Urano,[3] Mikiko Suzuki,[4] Takuya Iwami,[1] Katsuya Sato,[1] Masayuki Yamamoto,[5] Noriko Noguchi,[3] and Akira Kobayashi[1,2,7,*]

SUMMARY

Lipids, such as cholesterol and fatty acids, influence cell signaling, energy storage, and membrane formation. Cholesterol is biosynthesized through the mevalonate pathway, and aberrant metabolism causes metabolic diseases. The genetic association of a transcription factor NRF3 with obesity has been suggested, although the molecular mechanisms remain unknown. Here, we show that NRF3 upregulates gene expression in SREBP2-dependent mevalonate pathway. We further reveal that NRF3 overexpression not only reduces lanosterol, a cholesterol precursor, but also induces the expression of the *GGPS1* gene encoding an enzyme in the production of GGPP from farnesyl pyrophosphate (FPP), a lanosterol precursor. NRF3 overexpression also enhances cholesterol uptake through RAB5-mediated macropinocytosis process, a bulk and fluid-phase endocytosis pathway. Moreover, we find that GGPP treatment abolishes NRF3 knockdown-mediated increase of neutral lipids. These results reveal the potential roles of NRF3 in the SREBP2-dependent mevalonate pathway for cholesterol uptake through macropinocytosis induction and for lipogenesis inhibition through GGPP production.

INTRODUCTION

Lipids, including various insoluble biomolecules in water, are classified into several categories, such as fatty acids, glycerolipids, phospholipids, and sterol compounds (Fahy et al., 2005). Among them, cholesterol is the principal sterol of eukaryotic cells, such as yeast and mammalian cells, for signal transduction and membrane fluidity (Simons and Ikonen, 2000; Zinser et al., 1993). In mammals, cholesterol is derived from food and *de novo* biosynthesis. Dietary cholesterol in the blood is transported as part of a complex with low-density lipoproteins (LDLs) or high-density lipoproteins and is absorbed in the intestine (Lecerf and De Lorgeril, 2011). Hyperlipidemia, which refers to elevated lipid levels in the blood, is a higher risk of heart attack and stroke (Nelson, 2013). However, increased plasma cholesterol is further exacerbated by obesity and insulin resistance (Tabas, 2002). These insights suggest that high blood cholesterol levels are associated with cardiovascular and metabolic diseases. Also, cholesterol and fatty acids play an important role in cancer development, in which rapid growth of cancer cells is observed (Ding et al., 2019; Koundouros and Poulogiannis, 2020).

NF-E2-related factor 3 (NRF3) belongs to the cap'n'collar (CNC) family of transcription factors (Chowdhury et al., 2017; Kobayashi et al., 1999). The NRF3 protein binds to the endoplasmic reticulum (ER) membrane. Once the cells undergo stress or stimulation, such as proteasome inhibition, the NRF3 protein is cleaved by an aspartyl protease DNA-damage-inducible 1 homolog 2, which functions as a transcription factor with a heterodimer partner known as small Maf proteins (sMafs), including MafF, MafG, and MafK. Recently, we reported that NRF3 promotes the growth of human colorectal cancer HCT116 cells and induces the expression of several genes, such as the cell cycle regulator, *U2AF homology motif kinase 1* (*UHMK1*); proteasome assembly factor, *proteasome maturation protein* (*POMP*); and translational regulator, *cytoplasmic polyadenylation element-binding protein 3* (*CPEB3*) (Chowdhury et al., 2017; Waku et al, 2020a, 2020b). Additionally, genome-wide association studies from two independent groups have that association between a few loci near the *NRF3* gene might be associated with body mass index (BMI), although the statistical

[1]Laboratory for Genetic Code, Department of Medical Life Systems, Faculty of Life and Medical Sciences, Doshisha University, 1-3 Miyakodani, Tatara, Kyotanabe, Kyoto 610-0394, Japan

[2]Laboratory for Genetic Code, Graduate School of Life and Medical Sciences, Doshisha University, Kyotanabe, Kyoto 610-0394, Japan

[3]Systems Life Sciences Laboratory, Department of Medical Life Systems, Faculty of Life and Medical Sciences, Doshisha University, 1-3 Miyakodani, Tatara, Kyotanabe, Kyoto 610-0394, Japan

[4]Center for Radioisotope Sciences, Tohoku University Graduate School of Medicine, 2-1 Seiryo-cho, Aoba-ku, Sendai 980-8575 Japan

[5]Department of Medical Biochemistry, Tohoku University Graduate School of Medicine, 2-1 Seiryo-cho, Aoba-ku, Sendai 980-8575 Japan

[6]These authors contributed equally

[7]Lead contact

*Correspondence: akobayas@mail.doshisha.ac.jp

https://doi.org/10.1016/j.isci.2021.103180

significance is not observed (Lamiquiz-Moneo et al., 2019; Monda et al., 2013). However, it remains unclear whether and how NRF3 contributes to lipid metabolism and weight gain.

Sterol regulatory element-binding proteins (SREBPs) are membrane-bound transcription factors crucial for lipid metabolism (Brown and Goldstein, 1997; Horton et al., 2002). In vertebrates, SREBP1 and SREBP2 translocate from the ER to the Golgi apparatus in response to cholesterol depletion. Then, these proteins are processed by proteolytic cleavage and targeted to the nucleus. SREBP1 favors the gene expression of enzymes required for fatty acid biosynthesis and adipocyte differentiation, whereas SREBP2 is involved in the gene expression of enzymes required for cholesterol biosynthesis (Shimano, 2009). Thus, the orchestration of SREBP1 and SREBP2 is important to maintain appropriate cellular lipid metabolism.

Cholesterol is biosynthesized from acetyl-CoA through the mevalonate pathway. The mevalonate pathway is also responsible for the production of geranylgeranyl pyrophosphate (GGPP), which is metabolized from farnesyl pyrophosphate (FPP) by GGP synthase 1 (GGPS1). Similarly, GGPP functions as a required substrate for protein modification (geranylgeranylation), which serves as the lipophilic anchor and affects protein function and localization in membranes (Wang and Casey, 2016). Also among the proteins modified by GGPP, a Ras-related small GTPase protein, RAB5, is crucial for macropinocytosis, a bulk and fluid-phase endocytosis process (Feliciano et al., 2011; Zeigerer et al., 2012). Recently, it has been reported that pitavastatin leads to GGPP depletion and macropinocytosis inhibition (Jiao et al., 2020). Pitavastatin has been developed as an inhibitor of hydroxy-methylglutaryl-CoA reductase (HMGCR), which acts as a rate-limiting enzyme in cholesterol biosynthesis through the mevalonate pathway (Wensel et al., 2010). Therefore, these insights imply the biological relevance of the mevalonate pathway to macropinocytosis and cholesterol biosynthesis.

Here, we found that NRF3 upregulated gene expression in the SREBP2-dependent mevalonate pathway by inducing the expression of the *SREBP2* gene and forming a transcriptional complex with active SREBP2 proteins. We also identified *RAB5* and *GGPS1* as potential target genes of NRF3 and showed that NRF3 induced RAB5-mediated macropinocytosis for cholesterol uptake and GGPS1-mediated GGPP production for lipogenesis inhibition. Finally, we confirmed the upregulation of these gene expressions in Nrf3-transgenic (Nrf3-Tg) mouse colorectal tissues. Therefore, this study provides the gene expression network of NRF3-regulated lipid metabolism.

RESULTS

NRF3 upregulates gene expression in cholesterol biosynthesis through the mevalonate pathway

To investigate the NRF3-regulated gene expression network related to lipid metabolism, we performed a gene expression network analysis using DNA microarray data sets as follows: (1) human lung cancer H1299-NRF3 overexpressing (H1299-oeNRF3) cells compared with H1299-GFP overexpressing control (H1299-oeGFP) cells, and (2) human colon cancer HCT116-short interfering RNA (siRNA)-mediated NRF3 knockdown (HCT116-siNRF3) cells compared with HCT116-control siRNA knockdown (HCT116-siCont) cells. To exclude p53-dependent apoptosis induced by NRF3 knockdown, as reported previously (Waku et al., 2020b), we further performed (3) p53-deficient HCT116-siRNA-mediated NRF3 knockdown (p53KO HCT116-siNRF3) cells compared with p53KO HCT116-siCont knockdown (p53KO HCT116-siCont) cells. As a threshold, we used the fold change values for *POMP* and *UHMK1* genes because we have previously reported that the *POMP* gene was upregulated in H1299-oeNRF3 cells and that the *UHMK1* gene was downregulated by NRF3 knockdown in another human colorectal cancer, DLD-1 cells, without any stress or stimulation by NRF3 activation, such as a proteasome inhibition (Chowdhury et al., 2017; Waku et al., 2020b). We selected 1,517 upregulated genes at a fold change of ≥ 1.36 in H1299-oeNRF3 cells, 3,301 downregulated genes at a fold change of ≤ -1.26 in HCT116-siNRF3 cells, and 2,910 downregulated genes at a fold change of ≤ -1.22 in p53KO HCT116-siNRF3 cells. Venn diagram indicated 100 common genes among these selected genes (Figure 1A and Tables S1, S2, S3, and S4). After this step, cholesterol biosynthesis and isoprenoid biosynthesis (also known as the mevalonate pathway) were identified as the top and second annotation by gene ontology (GO) analysis of the 100 common genes (Figures 1B and 1C, Table S5). To validate these results, we performed real-time quantitative PCR (RT-qPCR) assays and confirmed that compared with GFP overexpression used as control, NRF3 overexpression induced the gene expression of enzymes required for cholesterol biosynthesis, including *hydroxy-methylglutaryl-CoA synthase 1 (HMGCS1), HMGCR, isopentenyl-diphosphate delta isomerase 1* (*IDI1*), and *methylsterol monooxygenase 1* (*MSMO1*) (Figures 1D and S1A). Consistent with this result, we observed that these gene expressions were suppressed in HCT116-siNRF3

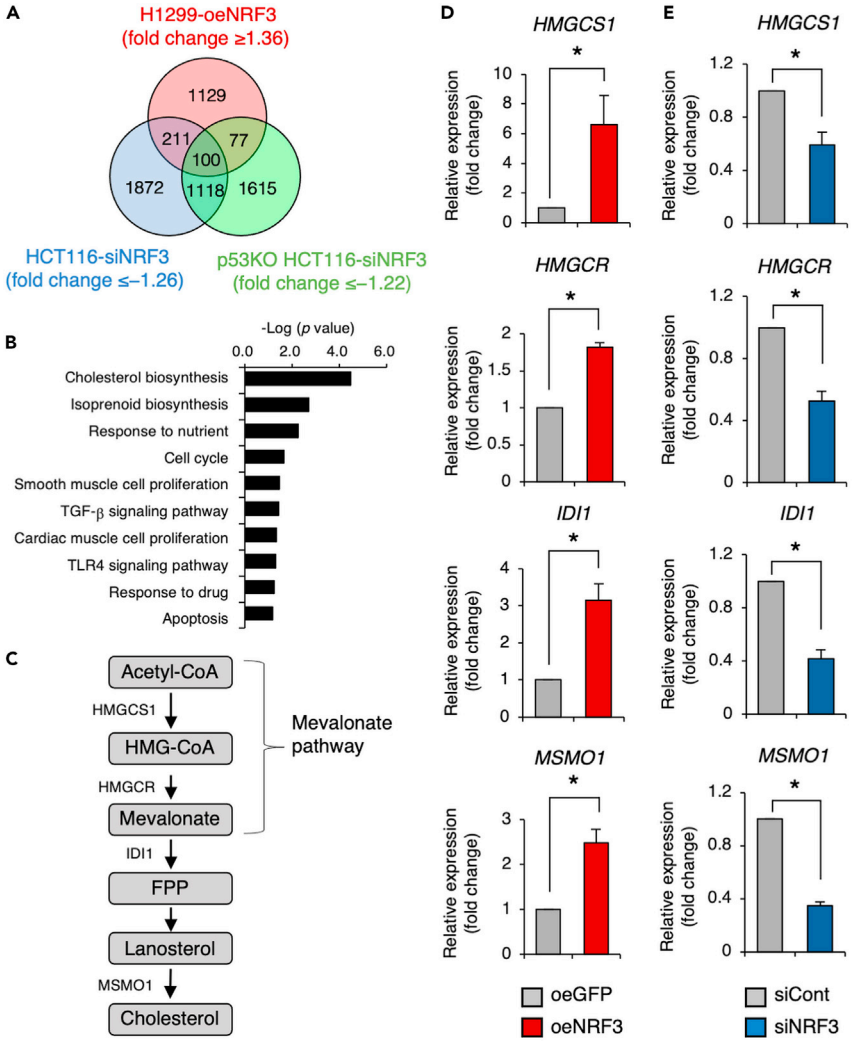

Figure 1. NRF3 induces the expression of five genes required for cholesterol biosynthesis

(A) Venn diagram of the up- or down-regulated gene sets in H1299-oeNRF3 cells (≥1.36-fold), HCT116-siNRF3 cells (≤−1.26-fold), and p53KO HCT116-siNRF3 cells (≤−1.22-fold).

(B) GO analysis of common 100 genes with up-regulated expression mediated by NRF3 overexpression and down-regulated by NRF3 knockdown.

(C) Regulated genes of *de novo* cholesterol biosynthesis through the mevalonate pathway.

(D and E) Effects of NRF3 overexpression or knockdown on the expression of five genes related to cholesterol biosynthesis in (C). H1299-oeNRF3 and H1299-oeGFP cells (D) or HCT116-siNRF3 and HCT116-siCont cells (E) were analyzed using RT-qPCR ($n = 3$). Mann–Whitney *U*-test: *p < 0.05. See also Figures S1A and S1B.

cells than in HCT116-siCont cells (Figures 1E and S1B). These results, therefore, indicate that NRF3 induces the gene expression of enzymes involved in cholesterol biosynthesis through the mevalonate pathway (Figure 1C).

SREBP2, a master regulator of cholesterol biosynthesis, is a potential target gene of NRF3

SREBP2 functions as a master transcriptional regulator of genes in *de novo* cholesterol biosynthesis, including *HMGCS1*, *HMGCR*, *IDI1*, and *MSMO1* (Xue et al., 2020). To investigate the functional correlation between NRF3 and SREBP2, we knocked down the *SREBP2* gene (Figure S1C) and found that SREBP2 knockdown significantly reduced these gene expressions without affecting NRF3 mRNA levels in H1299-oeNRF3 cells (Figure 2A, oeNRF3 + siCont *vs.* oeNRF3 + siSREBP2). Furthermore, RT-qPCR assays showed that the expression of the *SREBP2* gene was induced in H1299-oeNRF3 cells than in H1299-oeGFP cells (Figure 2A, oeGFP + siCont *vs.* oeNRF3 + siCont). Consistent results were obtained that the gene

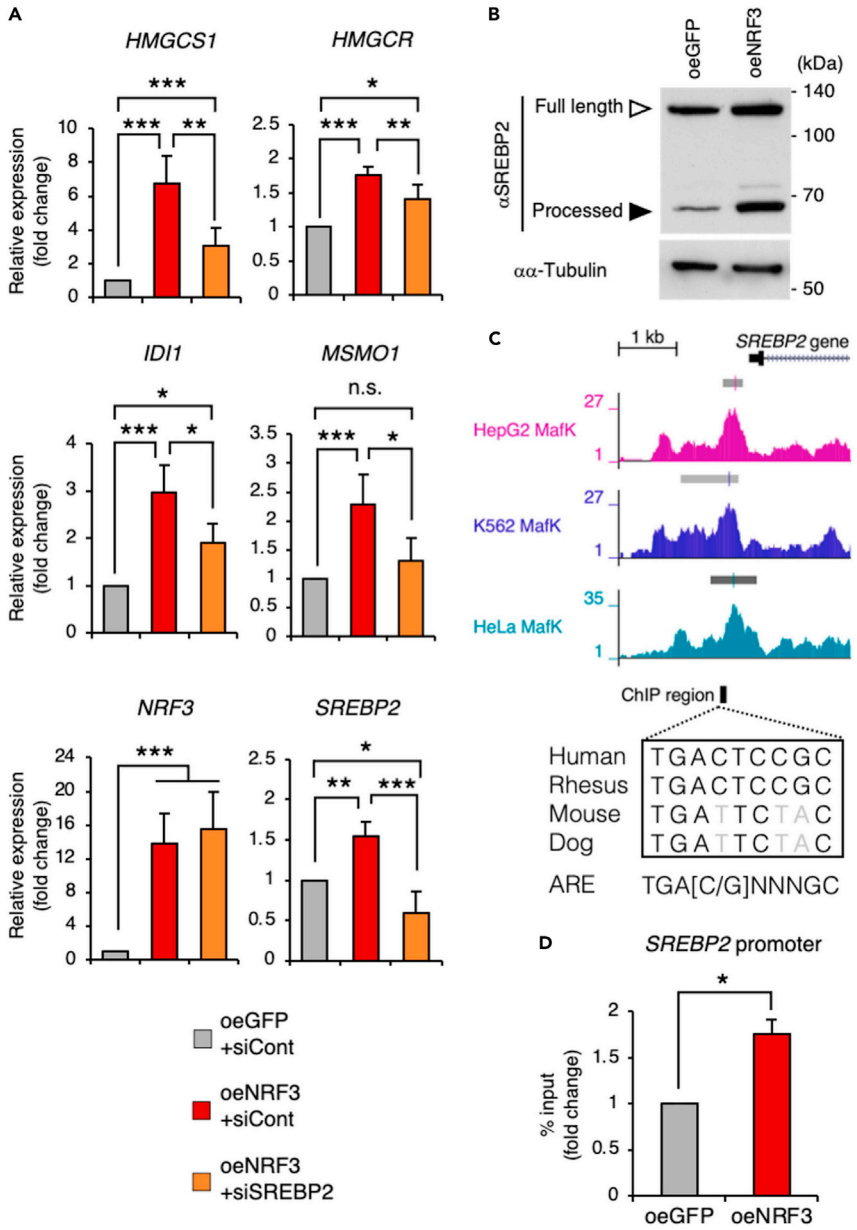

Figure 2. NRF3 induces gene expression and protein processing of SREBP2

(A) Effect of SREBP2 knockdown on the expression of the indicated genes in H1299-oeNRF3 cells. *SREBP2* gene was knocked down, after which the cells were analyzed using RT-qPCR. Control siRNA (siCont) was used as a negative control ($n = 4$).

(B) Effect of NRF3 overexpression on the protein processing of SREBP2. H1299-oeNRF3 and H1299-oeGFP cells were immunoblotted using the indicated antibodies.

(C and D) The recruitment of NRF3 on the *SREBP2* promoter in H1299-oeNRF3 and H1299-oeGFP cells. In (C), the genome locus of the *SREBP2* promoter at the human genome (GRCh37/hg19) is shown with previously generated ChIP-seq signals and peaks (gray rectangles) of MafK in indicated cell lines (Landt et al., 2012) and multiple sequences of a candidate ARE in indicated species using a web-tool UCSC Genome Browser (Kent et al., 2002). The region of ChIP-qPCR (ChIP region) is shown as a black rectangle at the bottom. In (D). H1299-oeNRF3 and H1299-oeGFP cells were treated with 1 μM MG-132 for 24 h and then analyzed using ChIP-qPCR ($n = 3$). (A) ANOVA followed by Tukey's test, (D) Mann–Whitney *U*-test: ***$p < 0.005$; **$p < 0.01$; *$p < 0.05$; n.s., not significant. See also Figures S1C and S2.

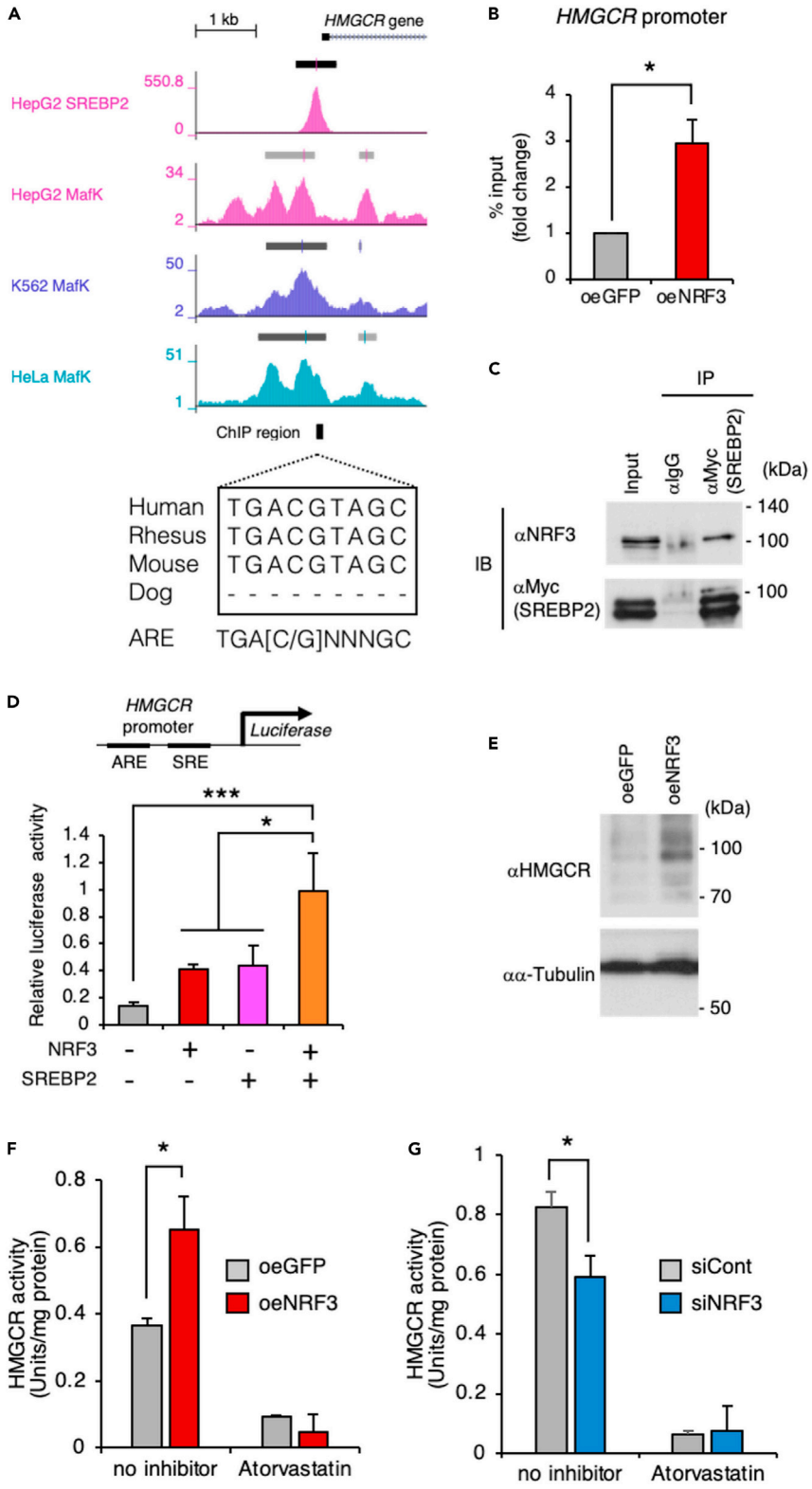

Figure 3. NRF3 interacts with SREBP2 for *HMGCR* gene expression

(A and B) The recruitment of NRF3 on the *HMGCR* promoter in H1299-oeNRF3 and H1299-oeGFP cells. In (A), the genome locus of the promoter at the human genome (GRCh37/hg19) is shown with previously generated ChIP-seq signals (color

Figure 3. *Continued*

bars) and peaks (gray rectangles) of SREBP2 and MafK in indicated cell lines (Landt et al., 2012) and multiple sequences of a candidate ARE in indicated species using a web-tool UCSC Genome Browser (Kent et al., 2002). In (B), H1299-oeNRF3 and H1299-oeGFP cells were treated with 1 μM MG-132 for 24 h and then analyzed using ChIP-qPCR (n = 3).

(C) The physical interaction between NRF3 and SREPB2 proteins. p3×FLAG-NRF3ΔNHB1 and p6×Myc-SREBP2ΔC was co-transfected into the HCT116 cells. At 24 h after co-transfection, the cells were subjected to Co-IP experiments using the indicated antibodies.

(D) Synergistic effect of NRF3 and SREBP2 on the transcription driven from the *HMGCR* promoter. A luciferase reporter vector fused with the promoter was co-transfected with indicated plasmid to HCT116 cells. At 24 h after co-transfection, the cells were subjected to the luciferase reporter assay (n = 3).

(E) Effect of NRF3 overexpression on HMGCR protein levels. H1299-oeNRF3 and H1299-oeGFP cells were immunoblotted using the indicated antibodies.

(F and G) Effect of NRF3 overexpression or knockdown on HMGCR activity. H1299-oeNRF3 and H1299-oeGFP cells (F) or HCT116-siNRF3 and HCT116-siCont cells (G) were analyzed (n = 3). An HMGCR inhibitor atorvastatin was used as a negative control. (B, F, G) Mann–Whitney U-test, (D) ANOVA followed by Tukey's test: ***$p < 0.005$; *$p < 0.05$. See also Figure S3.

expression was reduced in HCT116-siNRF3 cells than in HCT116-siCont cells (Figure S2A). Similarly, these results propose that NRF3 activates the SREBP2 pathway. We also found that the protein levels of processed SREBP2 proteins were increased in H1299-oeNRF3 cells than in H1299-oeGFP cells (Figure 2B). Consistent with this result, we observed that the processed proteins were decreased in HCT116-siNRF3 cells than in HCT116-siCont cells (Figure S2B). In the *SREBP2* promoter, the NRF3 binding region (also called as the antioxidant response element, ARE) is located in the previously generated chromatin immunoprecipitation-sequence (ChIP-seq) peak of MafK, an NRF3 heterodimer partner (Landt et al., 2012) (Figure 2C). Moreover, ChIP-qPCR assays also showed NRF3 recruitment onto the ChIP region containing the ARE in the *SREBP2* promoter (Figure 2D). These results, therefore, indicate that NRF3 directly induces the gene expression of *SREBP2* as well.

NRF3 and SREBP2 synergistically induce the gene expression of *HMGCR* encoding a rate-limiting enzyme in cholesterol biosynthesis

NRF3 overexpression significantly induced *HMGCS1*, *HMGCR*, and *IDI1* genes, even if *SREBP2* gene was knocked down (Figure 2A, oeGFP + siCont *vs.* oeNRF3 + siSREBP2). This result implies the possibility that these gene expressions are directly induced by NRF3 and SREBP2 as well. Previously generated ChIP-seq peaks of SREBP2 and MafK proteins were adjacent or overlapped in each gene promoter (Landt et al., 2012) (Figures 3A and S3). We also confirmed NRF3 recruitment onto the ChIP region contained in those peaks of SREBP2 and MafK in the *HMGCR* promoter (Figure 3B). These results propose that NRF3 and SREBP2 form a transcriptional complex that induces the expression of the *HMGCR* gene, encoding a rate-limiting enzyme in cholesterol biosynthesis. To address this issue, we examined the protein interaction between NRF3 and SREBP2 by co-immunoprecipitation (Co-IP) experiments. Full-length proteins of NRF3 are anchored in the ER membranes *via* its NHB1 (N-terminal homology box 1) domain in the N-terminus. Similarly, full-length SREBP2 proteins possess two transmembrane sequences in the C-terminus. The protein processing is essential for the transcriptional activation of NRF3 and SREBP2. Thus, we designed and constructed the expression plasmids of NRF3 lacking the NHB1 domain (NRF3ΔNHB1) and SREBP2 lacking the C-terminal region (SREBP2ΔC). Using these plasmids, we performed Co-IP experiments and found the interaction between NRF3ΔNHB1 and SREBP2ΔC (Figure 3C). Then, we investigated the cooperative transcriptional activity of NRF3 and SREBP2 using a luciferase reporter assay of the *HMGCR* promoter containing both ARE and SREBP2 binding regions (also called the sterol regulatory element, SRE). Co-expression of NRF3 and SREBP2 synergistically increased the reporter activity derived from the *HMGCR* promoter compared with the single transfection of either NRF3 or SREBP2 (Figure 3D).

NRF3 overexpression increased the protein levels of HMGCR (Figure 3E). Thus, we investigated whether NRF3 is crucial for HMGCR function. To address this issue, we performed the HMGCR activity assay based on the spectrophotometric measurement of the decrease in absorbance at 340 nm, representing the oxidation of NADPH by the catalytic subunit of HMGCR in the presence of HMG-CoA. As a result, the enzymatic activity of HMGCR was increased by NRF3 overexpression, while it was decreased by NRF3 knockdown (Figures 3F and 3G). These functional assay results agree with the expression levels of HMCGR mRNA and proteins. Altogether, these results indicate that NRF3 and SREBP2 proteins form a transcriptional complex for the synergistic induction of *HMGCR* gene expression, promoting the enzymatic activity.

NRF3 reprograms cholesterol biosynthesis to GGPP production by inducing *GGPS1* gene expression

Next, we investigated the impact of NRF3 on the intracellular levels of cholesterol and its precursor; lanosterol by gas chromatography–mass spectrometry (GC-MS) analysis. We hypothesized that NRF3 increases cholesterol levels by inducing the expression of genes related to cholesterol biosynthesis. Unexpectedly, NRF3 overexpression did not affect levels of cholesterol, even though it reduced levels of lanosterol, a precursor of cholesterol, compared with GFP overexpression (Figure 4A). Lanosterol is a precursor of cholesterol and a downstream metabolite of FPP, which is also metabolized to GGPP in a reaction catalyzed by GGPS1 (Figure 4B). We found that the expression of *GGPS1* gene was induced by NRF3 overexpression (Figure 4C) and obtained the consistent results that the gene expression was reduced by NRF3 knockdown (Figure S4). The genome browser shot also showed previously generated ChIP-seq peaks of sMaf in the *GGPS1* promoter (Landt et al., 2012) (Figure 4D). Therefore, we confirmed NRF3 recruitment onto the ChIP region contained in sMaf peaks in the *GGPS1* promoter (Figure 4E). These results thus imply that NRF3 directly induces the gene expression *GGPS1* and reprograms cholesterol biogenesis to the production of GGPP, rather than lanosterol.

NRF3 induces the gene expression of *RAB5* encoding an early endocytosis regulator

Then, we investigated the mechanism underlying the aforementioned unexpected results in which cholesterol levels were not changed, even though NRF3 overexpression reduced lanosterol levels (Figure 4A). The intracellular cholesterol is derived from not only *de novo* biosynthesis but also endocytic uptake. Thus, we hypothesized that NRF3 enhances endocytosis for cholesterol uptake to compensate for the potential depletion in cholesterol levels following lanosterol reduction. To address this issue, we investigated the impact of NRF3 on the expression of genes related to cholesterol uptake. Compared with GFP overexpression, NRF3 overexpression did not induce the gene expression of *LDL receptor* (*LDLR*) encoding a key regulator of LDL endocytosis (Figure 5A). We also observed no ARE within previously generated ChIP-seq peaks of SREBP2 and sMaf in the *LDLR* promoter (Landt et al., 2012) (Figure S5A), implying that *LDLR* is not important to NRF3-mediated cholesterol uptake. Meanwhile, NRF3 overexpression induced the gene expression of three isoforms of *Ras-related protein 5* (*RAB5A*, *RAB5B*, and *RAB5C*), each of which acts as an early endocytosis regulator (Zeigerer et al., 2012) (Figure 5B). In this study, we obtained consistent results that each *RAB5* gene was reduced in HCT116-siNRF3 cells than in HCT116-siCont cells (Figure S5B). Furthermore, we found previously generated ChIP-seq peaks of sMaf in the promoter of each *RAB5* gene (Landt et al., 2012) (Figure S5C) and confirmed NRF3 recruitment onto the ChIP region contained in sMaf peaks in each *RAB5* promoter (Figure S5D). We also confirmed that NRF3 overexpression increased the protein levels of RAB5 compared with GFP overexpression (Figure 5C). Since post-translational prenylation of RAB5 protein with GGPP is essential for proper localization and activation of these proteins (Alejandro Barbieri et al., 1998), we speculate that increased production of GGPP increased RAB5 prenylation. The results showed that prenylated RAB5 was increased in H1299-oeNRF3 cells compared with H1299-oeGFP cells (Figure 5D). These results propose the possibility that NRF3 enhances RAB5-mediated endocytosis rather than LDLR-mediated endocytosis for cholesterol uptake through GGPP production.

NRF3 enhances cholesterol uptake through RAB5-mediated macropinocytosis

RAB5 protein is a Ras-related small GTPase involved in macropinocytosis, a bulk and fluid-phase endocytosis process (Kruth et al., 2005). Next, we investigated the impact of NRF3 on the endocytic uptake of cholesterol through RAB5-mediated macropinocytosis. To address this issue, we performed an LDL uptake assay using a DyLight 488-labeled LDL (LDL-DyLight). Results showed that LDL-DyLight uptake was enhanced in H1299-oeNRF3 cells than in the wild-type H1299 (H1299-WT) cells (Figure 5E, WT *vs.* oeNRF3 in siCont). Furthermore, we used a mixture of siRNA oligonucleotides against each *RAB5* isoform (Figure S1D) and confirmed that NRF3-enhanced uptake of LDL-DyLight was abolished by the knockdown of all *RAB5* isoforms (Figure 5E, WT *vs.* oeNRF3 in siRAB5). We then used two indicators of macropinocytosis, fluorescein isothiocyanate (FITC)-labeled 70-kD dextran (FITC-Dextran) and bovine serum albumin (FITC-BSA). Results showed that the uptake of FITC-dextran and FITC-BSA was enhanced in the H1299-oeNRF3 cells than in the H1299-WT cells (Figure 5F, WT *vs.* oeNRF3). Furthermore, we confirmed that NRF3-enhanced uptake of each FITC indicator was abolished by treatment with 5-(N-ethyl-N-isopropyl)amiloride (EIPA), which is also known as an inhibitor of macropinocytosis and a selective blocker of Na^+/H^+ exchanger (Commisso et al., 2014) (Figure 5F, oeNRF3 *vs.* oeNRF3 + EIPA). Similar results were also obtained using two nitrobenzoxadiazole (NBD)-labeled cholesterols, such as the 25-NBD cholesterol and the NBD-12

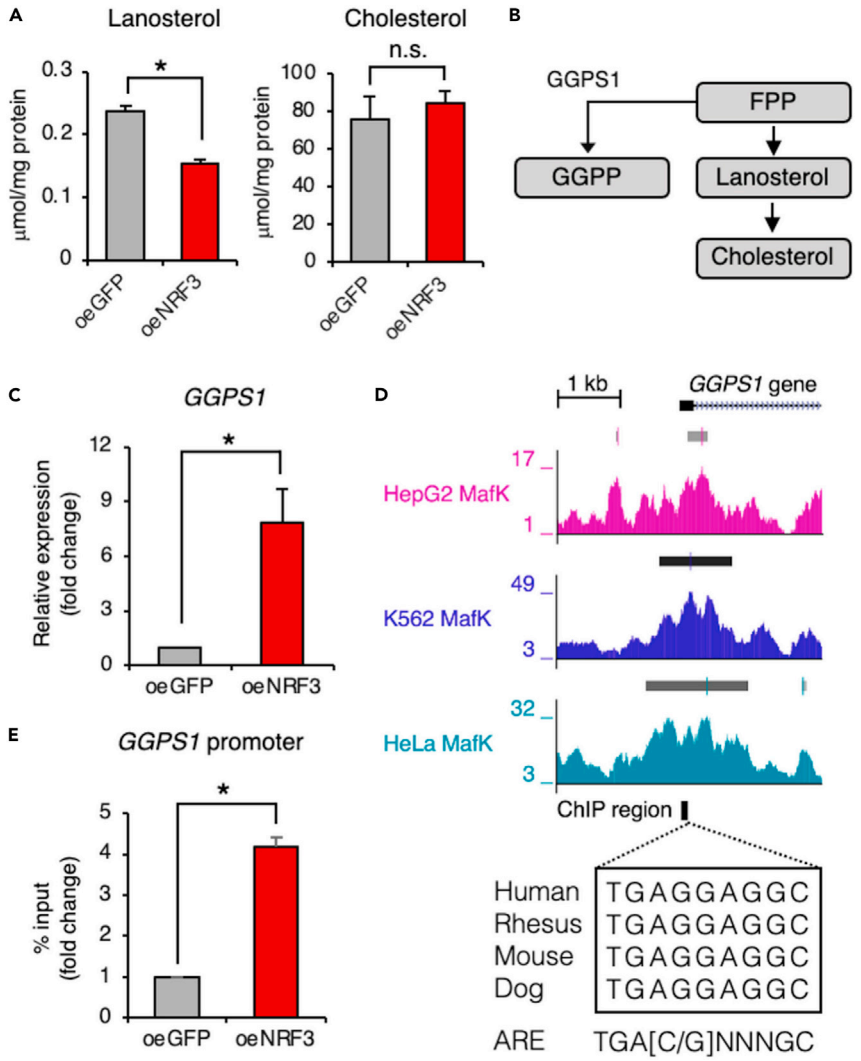

Figure 4. NRF3 reduces lanosterol levels and induces the gene expression of GGPS1

(A) Effect of NRF3 overexpression on intercellular levels of lanosterol (*top*) and cholesterol (*bottom*). H1299-oeNRF3 and H1299-oeGFP cells were subjected to GC-MS (n = 3).

(B) Reprogramming cholesterol biosynthesis to GGPP production by GGPS1.

(C) Effect of NRF3 overexpression on the expression of *GGPS1* gene (n = 3).

(D and E) The recruitment of NRF3 on the *GGPS1* promoter in H1299-oeNRF3 and H1299-oeGFP cells. In (D), the genome locus of the promoter at the human genome (GRCh37/hg19) is shown with the previously generated ChIP-seq signals and peaks (gray rectangles) of MafK in indicated cell lines (Landt et al., 2012) and multiple sequences of a candidate ARE in indicated species using a web-tool UCSC Genome Browser (Kent et al., 2002). The region of the ChIP-qPCR (ChIP region) is shown as a black rectangle at the bottom. In (E), H1299-oeNRF3 and H1299-oeGFP cells were treated with 1 μM MG-132 for 24 h and then analyzed using ChIP-qPCR (n = 3). (A, C, E) Mann–Whitney U-test: *$p < 0.005$; n.s., not significant. See also Figure S4.

cholesterol (Figure 5F). These results, therefore, indicate that NRF3 enhances cholesterol uptake through RAB5-mediated induction of macropinocytosis.

Lipogenesis inhibition is a potential role of NRF3-mediated GGPP production

We investigated the molecular mechanism and the biological significance of lanosterol reduction by NRF3. Previously, it has been reported that GGPP suppressed SREBP1-dependent fatty acid biosynthesis and intracellular lipid accumulation (Bertolio et al., 2019; Yeh et al., 2016), suggesting a possibility that NRF3 inhibited lipogenesis by inducing GGPP production. To address this issue, we performed a gene-set

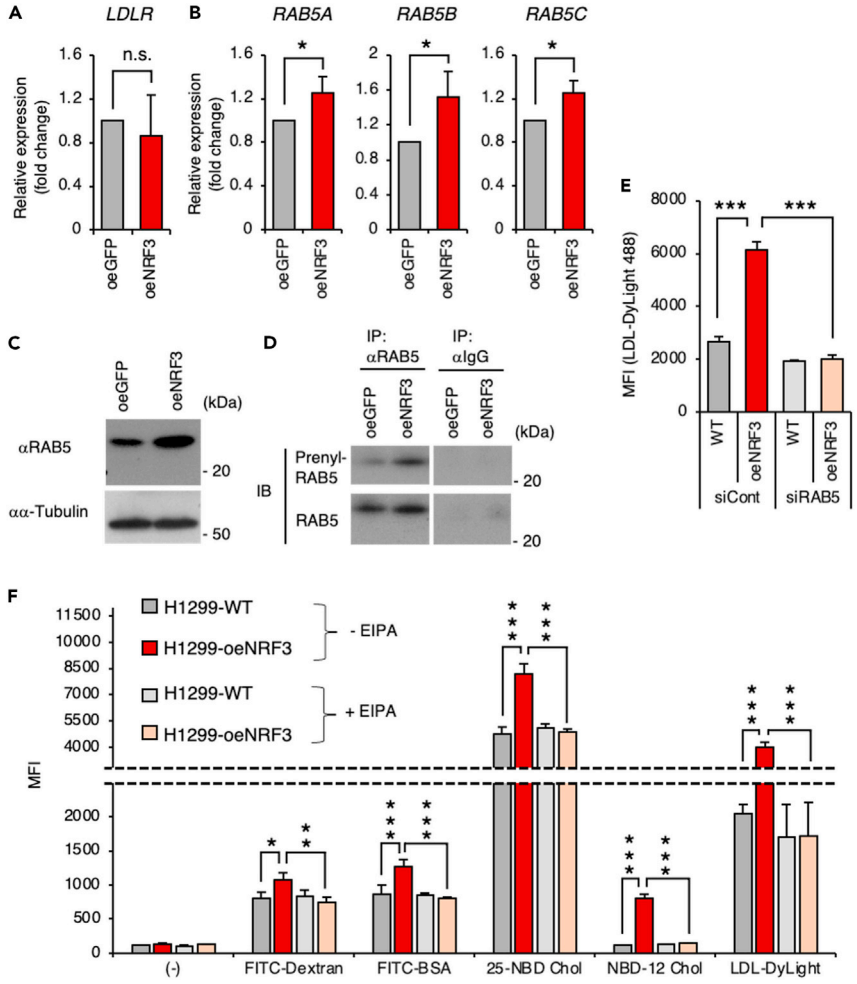

Figure 5. NRF3 induces RAB5-mediated macropinocytosis for cholesterol uptake

(A and B) Effect of NRF3 overexpression on the gene expression of *LDLR* (A) and three *RAB* isoforms (B) (n = 3).

(C) Effect of NRF3 overexpression on RAB5 protein levels. H1299-oeNRF3 and H1299-oeGFP cells were immunoblotted using antibodies that recognized all three RAB5 isoforms.

(D) Effect of NRF3 overexpression on RAB5 prenylation. H1299-oeNRF3 or oeGFP cells were subjected to Co-IP experiments using the indicated antibodies.

(E) Effects of NRF3 overexpression and RAB5 knockdown on LDL uptake in H1299-oeNRF3 (oeNRF3) or wild-type H1299 (WT) cells. All three *RAB5* isoforms were simultaneously knocked down, and then, the cells were labeled with LDL-DyLight 488.

(F) Effect of NRF3 overexpression on macropinocytosis. H1299-oeNRF3 and H1299-WT cells were incubated in the serum-free medium and then treated with the indicated indicator in the presence or absence of EIPA. In (E) and (F), median of fluorescent intensity (MFI) values of the indicated indicators are shown (n = 3). (A and B) Mann–Whitney U-test, (E and F) ANOVA followed by Tukey's test: ***p < 0.005; **p < 0.01; *p < 0.05; n.s., not significant. See also Figures S1D and S5.

enrichment analysis (GSEA) of H1299-oeNRF3 or HCT116-siCont cells. Results showed a negative correlation between the expression levels of *NRF3* and genes related to fatty acid metabolism (Figures 6A and 6B). In cells, fatty acids are converted to neutral lipids, including triacylglycerols, and sterol esters. Then, we stained neutral lipids in H1299-oeNRF3 or HCT116-siNRF3 cells with Nile red and quantified the fluorescence intensity of Nile red using flow cytometry. The fluorescence intensity was reduced in H1299-oeNRF3 cells than in H1299-WT cells (Figure 6C). We also obtained consistent results showing that the fluorescent intensity of Nile red was increased in HCT116-siNRF3 cells than in HCT116-siCont cells (Figure 6D, siCont *vs.* siNRF3). We further validated the impact of GGPP treatment on intracellular levels of neutral lipids in HCT116 cells and found that GGPP treatment reduced the intensity increased by NRF3 knockdown (Figure 6D, siNRF3 *vs.* siNRF3 + GGPP). These results, therefore, reveal the potential role of NRF3-mediated

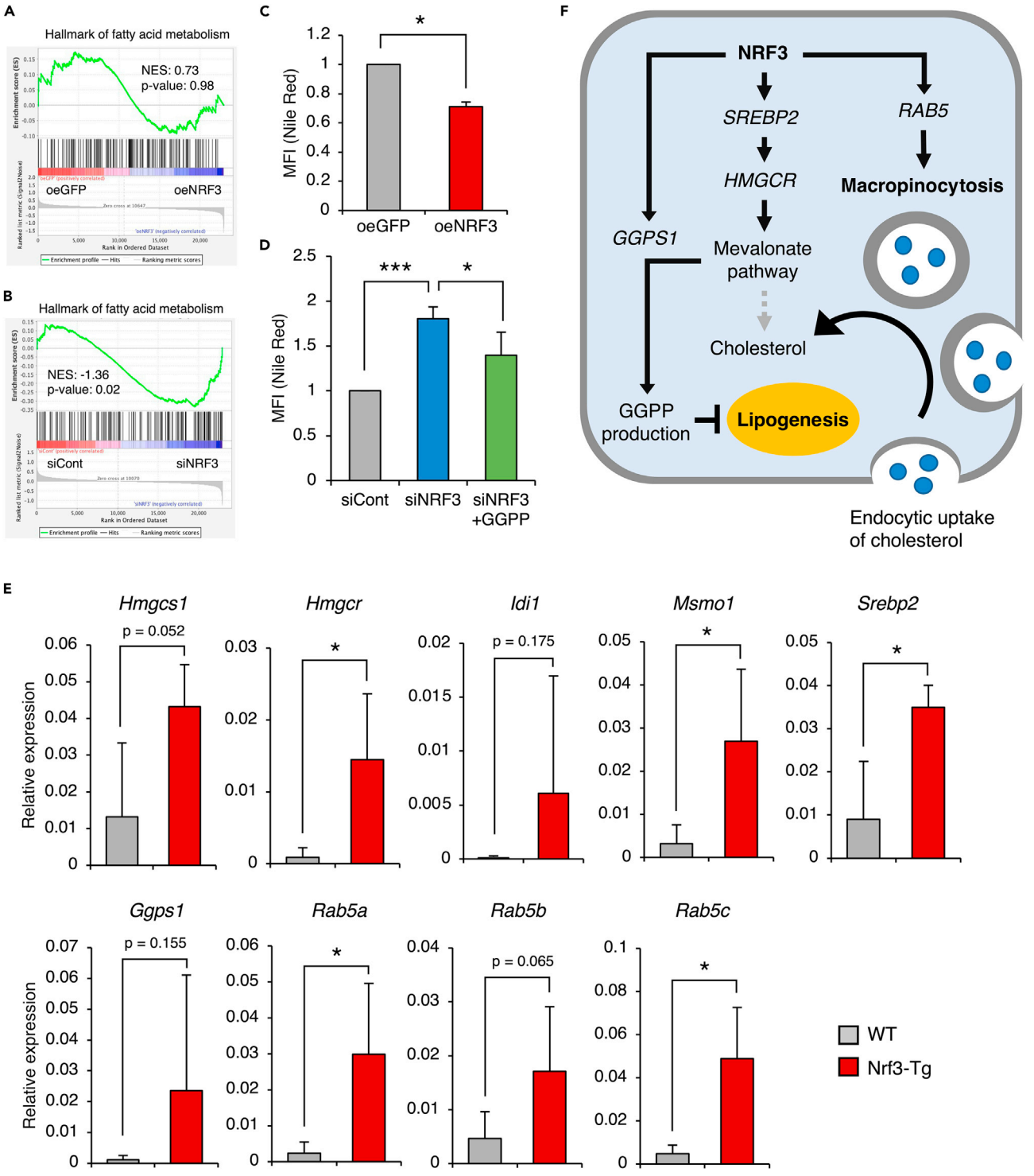

Figure 6. NRF3 reduces neutral lipid levels through GGPP production

(A and B) Enrichment plots of fatty acid metabolism. The x-axis shows the rank order of genes up-regulated in H1299-oeNRF3 cells (oeNRF3), compared with that in H1299-oeGFP cells (oeGFP) (A), or down-regulated in HCT116-siNRF3 cells (siNRF3), compared with that in HCT116-siCont (siCont) cells (B). The barcode indicates the position of related genes in the ranking list. The y-axis shows the distribution of the running enrichment score generated by walking down the list of ranked genes. Normalized enrichment score (NES) and nominal p values (p value) are shown in each plot.

Figure 6. *Continued*

(C and D) Effect of NRF3 and/or GGPP on intercellular levels of neutral lipids. H1299-oeNRF3 and H1299-oeGFP cells (C) or HCT116-siNRF3 and HCT116-siCont cells (D) were stained with Nile red. In (D), at 24 h after siRNA transfection, the cells were placed in a normal culture medium with 10 μM GGPP (Cayman) for 3 days. Median of fluorescent intensity (MFI) values of Nile red are shown (n = 3).

(E) Effect of Nrf3 overexpression on indicated gene expression in Nrf3-Tg mouse rectal tissue. Means and two independent values are represented as bars and marks, respectively (n = 3–4). Wild-type (WT) littermate mice were used as a negative control.

(F) A possible mechanism of NRF3-regulated lipid metabolism. NRF3 up-regulates gene expression in the SREPB2-dependent mevalonate pathway. Furthermore, NRF3 reprograms cholesterol biosynthesis to GGPP production and reduces neutral lipids through GGPS1-mediated GGPP production. NRF3 also enhances endocytic uptake of cholesterol through RAB5-mediated macropinocytosis induction. The increased cholesterol uptake can compensate for the decrease in cholesterol levels due to the diverted metabolism of lanosterol to GGPP. See also the Discussion section. (C) Mann–Whitney U-test, (D) ANOVA followed by Tukey's test, (E) Welch's t test: ***, $p < 0.005$; *, $p < 0.05$. See also Figures S1E and S1F, and S6.

GGPP production in lipogenesis inhibition, where NRF3 induces the expression of the *GGPS1* gene, reducing neutral lipids through GGPP production. We do not exclude other functions of NRF3-mediated GGPP production.

NRF3-mediated gene expression related to lipid metabolism is upregulated in colorectal tissues

To validate the *in vivo* function of NRF3 in gene expression shown using human colorectal cancer HCT116 cells in this study, we generated Nrf3-Tg mouse and performed RT-qPCR using the mouse colon and rectal tissues where Nrf3 was overexpressed (Figures S1E and S1F). In the rectal tissue, Nrf3 induced the expression of genes related to cholesterol biosynthesis, including *Hmgcs1*, *Hmgcr*, *Idi1*, *Msmo1*, and *Srebp2*. Furthermore, we found an increase in the gene expression of *Ggps1* and three *Rab5* isoforms (Figure 6E). Consistent results were also obtained in the colon tissue (Figure S6). Although all gene inductions have not always been statistically significant, these results suggest the critical role of Nrf3 in colorectal tissues for lipid metabolism with GGPP production and micropinocytosis induction.

DISCUSSION

In this study, we propose the gene expression network of NRF3-mediated regulation of the SREBP2-dependent mevalonate pathway with cholesterol uptake and lipogenesis inhibition. NRF3 induces gene expression of *SREBP2* and enzymes required for cholesterol biosynthesis through the mevalonate pathway. NRF3 further leads to SREBP2 activation through the direct induction of gene expression. NRF3 and SREBP2 synergistically induce the gene expression of *HMGCR*, a rate-limiting enzyme in the mevalonate pathway. In addition to the upregulation of the SREBP2-dependent mevalonate pathway, NRF3 has potential roles in the RAB5-mediated induction of macropinocytosis for cholesterol uptake and the GGPS1-mediated reprogramming of cholesterol biosynthesis to GGPP production for lipogenesis inhibition (Figure 6F). Furthermore, we confirmed the *in vivo* function of NRF3 in gene expression in mouse colorectal tissues. In the following paragraphs, we discuss not only the pathophysiological aspects of the current findings on obesity and cancer development but also other mechanisms related to these NRF3 functions.

A few BMI-associated genomic loci near the *NRF3* gene have been identified previously (Lamiquiz-Moneo et al., 2019; Monda et al., 2013), although it remains unclear whether NRF3 contributes to adiposity. In this study, we showed that NRF3 and SREBP2 formed a transcriptional complex for the synergistic induction of the *HMGCR* gene expression, promoting the enzymatic activity (Figure 3). Against our expectation, cholesterol levels were not changed whereas lanosterol levels were decreased (Figures 4A and 4B). It was also found that NRF3 induced *GGPS1* gene expression (Figures 4C and S4) and that the accumulation of neutral lipids observed in siNRF3 cells was abolished by the addition of GGPP (Figure 6D). These results propose the following possibility: NRF3 reprograms the mevalonate pathway to the production of GGPP, rather than lanosterol through the direct induction of *GGPS1* gene expression. This potential role of NRF3 for GGPP production further leads to lipogenesis inhibition. Taken together, these results propose NRF3 deficiency as a risk factor for obesity.

In addition to obesity, our findings provide interesting insights into cancer development. Metabolic reprogramming toward increasing the mevalonate pathway activity enhances epithelial–mesenchymal transition and stemness of cancer cells (Mullen et al., 2016). Also, macropinocytosis inhibition leads to starvation and death of the cancer cells with oncogenic defects, including *PTEN* deficiency and *K-Ras*^{G12V} mutation (Jiao et al., 2020). We previously reported that *APC* deficiency, another well-known oncogenic defect, induces aberrant expression of the *NRF3* gene, resulting in tumorigenesis, metastasis, and

poor prognosis (Aono et al., 2019; Kobayashi and Waku, 2020). Oncogenic defect, such as *PTEN* deficiency, *K-Ras*^{G12V} mutation, and *APC* deficiency, causes rapid growth and metastasis of tumor. Furthermore, *in vivo* experiments using an Nrf3-Tg mouse suggested the crucial roles of Nrf3 for the SREBP2-dependent mevalonate pathway with cholesterol absorption and lipogenesis in the colon and rectal tissues (Figures 6E and S6). The meta-analysis of the previously reported prospective studies showed that dyslipidemia, especially high serum triglyceride, and total cholesterol levels, is associated with an increased risk of colorectal cancer (Yao and Tian, 2015). Therefore, these insights propose that a gene expression network of NRF3-regulated lipid metabolism through the mevalonate pathway and macropinocytosis induction is the potential mechanism underlying colorectal cancer development.

Several reports help us understand the molecular mechanism behind SREBP2 activation through NRF3-induced expression of the gene. In the ER membranes, SREBP2 proteins bind to SREBP cleavage-activating protein (SCAP) and insulin-inducing gene (INSIG) proteins (Yang et al., 2002a, 2002b). When cellular cholesterol levels are reduced, SREBP2/SCAP complex is released from the INSIG protein in the ER membrane and is then transported to the Golgi apparatus where two proteases sequentially cleave and activate the SREBP2 proteins. It has been reported that SREBP2 overexpression leads to protein processing (Yang et al., 2002b). These insights propose that NRF3-induced expression of the *SREBP2* gene leads to an excess of SREBP2 proteins and the increase in SREBP2 proteins unbound with INSIG proteins. Therefore, aberrant dissociation of the SREBP2/SCAP complex to INSIG proteins was enhanced by NRF3 overexpression, resulting in protein processing and activation of SREBP2 beyond transcriptional regulation.

Next, we discussed the possible mechanism underlying lipogenesis inhibition through NRF3-mediated GGPP production. Recently, it has been reported how GGPP inhibits SREBP1 and fatty acid biosynthesis (Bertolio et al., 2019). GGPP treatment increases geranylgeranylated RhoA, which is a Ras-related small GTPase protein similar to RAB5. Upon geranylgeranylation, RhoA localizes at the plasma membrane and triggers actin polymerization and actomyosin contraction, which has a key role in mechanosensing of the architecture and rigidity of the extracellular matrix (ECM). Actomyosin contraction is crucial for the activation of AMP-activated protein kinase (AMPK), which inhibits the activation of SREBP1 (Li et al., 2011). Thus, geranylgeranylated RhoA-mediated actomyosin contraction inhibits SREBP1-dependent lipid biosynthesis through AMPK activation in response to ECM stiffness. These insights propose that NRF3 increases geranylgeranylation of RhoA and inhibits SREBP1-dependent lipogenesis through GGPP production.

Our findings also showed the impact of NRF3-mediated induction observed more pronouncedly at the protein levels of RAB5 (Figure 5C) and on endocytic uptake (Figures 5E and 5F) compared with the mRNA levels of RAB5 isoforms (Figure 5B). We have previously reported that NRF3 induced the expression of the *CPEB3* gene (Waku et al., 2020a). CPEB3 is a member of the CPEB-family, which are essential RNA-binding proteins of post-transcriptional gene expression with functions, including polyadenylation and ribosome recruitment onto mRNA (Fernández-Miranda and Méndez, 2012). In yeast, the expression of the *Ypt53* gene, a *RAB5* ortholog, is regulated by post-transcriptional mechanisms related to mRNA adenylation (Schmidt et al., 2017). Notably, we revealed that NRF3 increased RAB5 prenylation, which is crucial for endocytosis (Li et al., 1994) (Figure 5D). These insights imply additional effects of NRF3 on RAB5 function beyond its transcriptional upregulation.

Although the transcription activation factor, NRF3, is experimentally induced by treatment with proteasome inhibitors, such as MG-132, the endogenous cue of NRF3 activation remains unknown. Previously, it has been reported that NF-E2-related factor 1 (NRF1), the closest homolog of NRF3 in the CNC family, responds to cholesterol depletion in the ER membranes by directly binding to cholesterol through a cholesterol recognition amino-acid consensus motif domain (CRAC, L/V-$_{x1-5}$-Y-$_{x1-5}$-R/K) (Widenmaier et al., 2017). The CRAC domain is conserved in NRF3 proteins (Zhang et al., 2009). Taken together, our findings propose the possibility that cholesterol levels in the ER membrane are the endogenous cue of NRF3 activation. In other words, NRF3 functions as a cholesterol sensor similar to NRF1.

Limitations of the study

This study is limited to cell-based *in vitro* experiments and *in vivo* validation of gene expression. Therefore, it is critical to investigate whether our findings contribute to the phenotype, such as obesity and cancer. Future studies should also clarify the impact of NRF3-mediated GGPP production on SREBP1 inhibition

and geranylgeranylation and identify other target proteins of geranylgeranylation through NRF3-mediated GGPP production. In addition, we should confirm whether NRF3 function is modulated in response to cholesterol, and whether NRF3 increases the cellular amount of GGPP.

STAR★METHODS

Detailed methods are provided in the online version of this paper and include the following:

- KEY RESOURCES TABLE
- RESOURCE AVAILABILITY
  - Lead contact
  - Materials availability
  - Data and code availability
- EXPERIMENTAL MODEL AND SUBJECT DETAILS
  - Cell lines
  - Generation of Nrf3-Tg mouse
- METHOD DETAILS
  - Transfection
  - RNA extraction and RT-qPCR
  - DNA microarray analysis
  - Immunoblot analysis
  - Co-IP experiments
  - ChIP-qPCR
  - Luciferase reporter assays
  - GC-MS
  - Nile red staining
  - LDL uptake assay
  - Macropinocytosis assay
  - HMGCR activity assay
- QUANTIFICATION AND STATISTICAL ANALYSIS

SUPPLEMENTAL INFORMATION

Supplemental information can be found online at https://doi.org/10.1016/j.isci.2021.103180.

ACKNOWLEDGMENTS

We thank Ms. Yue Gao, Mr. Shuto Deguchi, Ms. Mika Matsumoto, Ms. Mika Fukumoto, and Ms. Hiromi Suda for the experimental supports. The pTK-HSV-BP2 plasmid was a gift from Dr. Juro Sakai (The University of Tokyo, Tohoku University). The pCAG-GFP plasmid was a gift from Dr. Saturu Takahashi (University of Tsukuba). This work was supported in part by a grant-in-aid for Scientific Research (C) (19K07650 to T.W., 19K07093 to Y.U); grant-in-aid from the Harris Research Institute of Doshisha University (to T.W. and Y.U.); grant-in-aid for Scientific Research (B) (16H03265, 20H04135 to A.K.); grant-in-aid for Challenging Research (Exploratory) (19K22826, 21K19743 to A.K.); and grant-in-aid from the Mitsubishi Foundation (to A.K.).

AUTHOR CONTRIBUTIONS

Conceptualization, T.W., T.H., N.T., Y.A., and Y.U.; validation and investigation, T.W., T.H., N.T., Y.A., T.I., and K.S.; generation of Nrf3-Tg mouse, M.S., M.Y., and A.K.; writing – original draft and visualization, T.W.; writing – review & editing, Y.U., N.N., and A.K.

DECLARATION OF INTERESTS

The authors declare no competing interests.

Received: April 30, 2021
Revised: September 18, 2021
Accepted: September 22, 2021
Published: October 22, 2021

REFERENCES

Ainoya, K., Moriguchi, T., Ohmori, S., Souma, T., Takai, J., Morita, M., Chandler, K.J., Mortlock, D.P., Shimizu, R., Engel, J.D., et al. (2012). UG4 enhancer-driven GATA-2 and bone morphogenetic protein 4 complementation remedies the CAKUT phenotype in Gata2 hypomorphic mutant mice. Mol. Cell. Biol. *32*, 2312–2322. https://doi.org/10.1128/mcb.06699-11.

Alejandro Barbieri, M., Hoffenberg, S., Roberts, R., Mukhopadhyay, A., Pomrehn, A., Dickey, B.F., and Stahl, P.D. (1998). Evidence for a symmetrical requirement for rab5-GTP in in vitro endosome-endosome fusion. J. Biol. Chem. *273*, 25850–25855. https://doi.org/10.1074/JBC.273.40.25850.

Aono, S., Hatanaka, A., Hatanaka, A., Gao, Y., Hippo, Y., Taketo, M.M., Waku, T., and Kobayashi, A. (2019). β-catenin/TCF4 complex-mediated induction of the NRF3 (NFE2L3) gene in cancer cells. Int. J. Mol. Sci. *20*, 3344. https://doi.org/10.3390/ijms20133344.

Bertolio, R., Napoletano, F., Mano, M., Maurer-Stroh, S., Fantuz, M., Zannini, A., Bicciato, S., Sorrentino, G., and Del Sal, G. (2019). Sterol regulatory element binding protein 1 couples mechanical cues and lipid metabolism. Nat. Commun. *10*, 1326.

Brown, M.S., and Goldstein, J.L. (1997). The SREBP pathway: regulation of cholesterol metabolism by proteolysis of a membrane-bound transcription factor. Cell *89*, 331–340. https://doi.org/10.1016/S0092-8674(00)80213-5.

Chowdhury, A.M.M.A., Katoh, H., Hatanaka, A., Iwanari, H., Nakamura, N., Hamakubo, T., Natsume, T., Waku, T., and Kobayashi, A. (2017). Multiple regulatory mechanisms of the biological function of NRF3 (NFE2L3) control cancer cell proliferation. Sci. Rep. *7*, 12494. https://doi.org/10.1038/s41598-017-12675-y.

Commisso, C., Flinn, R.J., and Bar-Sagi, D. (2014). Determining the macropinocytic index of cells through a quantitative image-based assay. Nat. Protoc. *9*, 182–192. https://doi.org/10.1038/nprot.2014.004.

Ding, X., Zhang, W., Li, S., and Yang, H. (2019). The role of cholesterol metabolism in cancer. Am. J. Cancer Res. *9*, 219–227.

Fahy, E., Subramaniam, S., Brown, H.A., Glass, C.K., Merrill, A.H., Murphy, R.C., Raetz, C.R.H., Russell, D.W., Seyama, Y., Shaw, W., et al. (2005). A comprehensive classification system for lipids. J. Lipid Res. *46*, 839–861. https://doi.org/10.1194/jlr.E400004-JLR200.

Feliciano, W.D., Yoshida, S., Straight, S.W., and Swanson, J.A. (2011). Coordination of the Rab5 cycle on macropinosomes. Traffic *12*, 1911–1922. https://doi.org/10.1111/j.1600-0854.2011.01280.x.

Fernández-Miranda, G., and Méndez, R. (2012). The CPEB-family of proteins, translational control in senescence and cancer. Ageing Res. Rev. *11*, 460–472. https://doi.org/10.1016/J.ARR.2012.03.004.

Horton, J.D., Goldstein, J.L., and Brown, M.S. (2002). SREBPs: activators of the complete program of cholesterol and fatty acid synthesis in the liver. J. Clin. Invest. *109*, 1125–1131. https://doi.org/10.1172/JCI0215593.

Hua, X., Sakai, J., Brown, M.S., and Goldstein, J.L. (1996). Regulated cleavage of sterol regulatory element binding proteins requires sequences on both sides of the endoplasmic reticulum membrane. J. Biol. Chem. *271*, 10379–10384. https://doi.org/10.1074/jbc.271.17.10379.

Huang, D.W., Sherman, B.T., and Lempicki, R.A. (2009). Bioinformatics enrichment tools: paths toward the comprehensive functional analysis of large gene lists. Nucl. Acids Res. *27*, 1–13. https://doi.org/10.1093/nar/gkn923.

Jiao, Z., Cai, H., Long, Y., Sirka, O.K., Padmanaban, V., Ewald, A.J., and Devreotes, P.N. (2020). Statin-induced GGPP depletion blocks macropinocytosis and starves cells with oncogenic defects. Proc. Natl. Acad. Sci. U S A *117*, 4158–4168. https://doi.org/10.1073/pnas.1917938117.

Kent, W.J., Sugnet, C.W., Furey, T.S., Roskin, K.M., Pringle, T.H., Zahler, A.M., and Haussler, a.D. (2002). The human genome browser at UCSC. Genome Res. *12*, 996–1006. https://doi.org/10.1101/gr.229102.

Kobayashi, A., Ito, E., Toki, T., Kogame, K., Takahashi, S., Igarashi, K., Hayashi, N., and Yamamoto, M. (1999). Molecular cloning and functional characterization of a new Cap'n' collar family transcription factor Nrf3. J. Biol. Chem. *274*, 6443–6452. https://doi.org/10.1074/jbc.274.10.6443.

Kobayashi, A., and Waku, T. (2020). New addiction to the NRF2-related factor NRF3 in cancer cells: ubiquitin-independent proteolysis through the 20S proteasome. Cancer Sci. *111*, 6–14. https://doi.org/10.1111/cas.14244.

Koundouros, N., and Poulogiannis, G. (2020). Reprogramming of fatty acid metabolism in cancer. Br. J. Cancer *122*, 4–22. https://doi.org/10.1038/s41416-019-0650-z.

Kruth, H.S., Jones, N.L., Huang, W., Zhao, B., Ishii, I., Chang, J., Combs, C.A., Malide, D., and Zhang, W.Y. (2005). Macropinocytosis is the endocytic pathway that mediates macrophage foam cell formation with native low density lipoprotein. J. Biol. Chem. *280*, 2352–2360. https://doi.org/10.1074/jbc.M407167200.

Lamiquiz-Moneo, I., Mateo-Gallego, R., Bea, A.M., Dehesa-García, B., Pérez-Calahorra, S., Marco-Benedí, V., Baila-Rueda, L., Laclaustra, M., Civeira, F., and Cenarro, A. (2019). Genetic predictors of weight loss in overweight and obese subjects. Sci. Rep. *9*, 10770. https://doi.org/10.1038/s41598-019-47283-5.

Landt, S.G., Marinov, G.K., Kundaje, A., Kheradpour, P., Pauli, F., Batzoglou, S., Bernstein, B.E., Bickel, P., Brown, J.B., Cayting, P., et al. (2012). ChIP-seq guidelines and practices of the ENCODE and modENCODE consortia. Genome Res. *22*, 1813–1831. https://doi.org/10.1101/GR.136184.111.

Lecerf, J.M., and De Lorgeril, M. (2011). Dietary cholesterol: from physiology to cardiovascular risk. Br. J. Nutr. *106*, 6–14. https://doi.org/10.1017/S0007114511000237.

Li, G., Barbieri, M.A., Colombo, M.I., and Stahl, P.D. (1994). Structural features of the GTP-binding defective Rab5 mutants required for their inhibitory activity on endocytosis. J. Biol. Chem. *269*, 14631–14635. https://doi.org/10.1016/S0021-9258(17)36671-1.

Li, Q., Zhang, H., Zou, J., Feng, X., and Feng, D. (2019). Bisphenol A induces cholesterol biosynthesis in HepG2 cells via SREBP-2/HMGCR signaling pathway. J. Toxicol. Sci. *44*, 481–491. https://doi.org/10.2131/JTS.44.481.

Li, Y., Xu, S., Mihaylova, M.M., Zheng, B., Hou, X., Jiang, B., Park, O., Luo, Z., Lefai, E., Shyy, J.Y.J., et al. (2011). AMPK phosphorylates and inhibits SREBP activity to attenuate hepatic steatosis and atherosclerosis in diet-induced insulin-resistant mice. Cell Metab. *13*, 376–388. https://doi.org/10.1016/j.cmet.2011.03.009.

Monda, K.L., Chen, G.K., Taylor, K.C., Palmer, C., Edwards, T.L., Lange, L.A., Ng, M.C.Y., Adeyemo, A.A., Allison, M.A., Bielak, L.F., et al. (2013). A meta-analysis identifies new loci associated with body mass index in individuals of African ancestry. Nat. Genet. *45*, 690–696. https://doi.org/10.1038/ng.2608.

Mootha, V.K., Lindgren, C.M., Eriksson, K.F., Subramanian, A., Sihag, S., Lehar, J., Puigserver, P., Carlsson, E., Ridderstråle, M., Laurila, E., et al. (2003). PGC-1α-responsive genes involved in oxidative phosphorylation are coordinately downregulated in human diabetes. Nat. Genet. *34*, 267–273. https://doi.org/10.1038/ng1180.

Mullen, P.J., Yu, R., Longo, J., Archer, M.C., and Penn, L.Z. (2016). The interplay between cell signalling and the mevalonate pathway in cancer. Nat. Rev. Cancer *16*, 718–731. https://doi.org/10.1038/nrc.2016.76.

Nelson, R. (2013). Hyperlipidemia as a risk factor for cardiovascular disease. Prim. Care *40*, 195–211. https://doi.org/10.1016/J.POP.2012.11.003.

Schmidt, O., Weyer, Y., Fink, M.J., Müller, M., Weys, S., Bindreither, M., and Teis, D. (2017). Regulation of Rab5 isoforms by transcriptional and post-transcriptional mechanisms in yeast. FEBS Lett. *591*, 2803–2815. https://doi.org/10.1002/1873-3468.12785.

Shimano, H. (2009). SREBPs: physiology and pathophysiology of the SREBP family. FEBS J. *276*, 616–621. https://doi.org/10.1111/j.1742-4658.2008.06806.x.

Simons, K., and Ikonen, E. (2000). How cells handle cholesterol. Science *290*, 1721–1726. https://doi.org/10.1126/science.290.5497.1721.

Subramanian, A., Tamayo, P., Mootha, V.K., Mukherjee, S., Ebert, B.L., Gillette, M.A., Paulovich, A., Pomeroy, S.L., Golub, T.R., Lander, E.S., et al. (2005). Gene set enrichment analysis: a knowledge-based approach for interpreting genome-wide expression profiles. Proc. Natl. Acad. Sci. U S A *102*, 15545–15550. https://doi.org/10.1073/pnas.0506580102.

Tabas, I. (2002). Cholesterol in health and disease. J. Clin. Invest. *110*, 583–590. https://doi.org/10.1172/JCI0216381.

Waku, T., Katayama, H., Hiraoka, M., Hatanaka, A., Nakamura, N., Tanaka, Y., Tamura, N., Watanabe, A., and Kobayashi, A. (2020a). NFE2L1 and NFE2L3 complementarily maintain basal proteasome activity in cancer cells through CPEB3-mediated translational repression. Mol. Cell. Biol. *40*, e00010–e00020. https://doi.org/10.1128/mcb.00010-20.

Waku, T., Nakamura, N., Koji, M., Watanabe, H., Katoh, H., Tatsumi, C., Tamura, N., Hatanaka, A., Hirose, S., Katayama, H., et al. (2020b). NRF3-POMP-20S proteasome assembly axis promotes cancer development via ubiquitin-independent proteolysis of p53 and retinoblastoma protein. Mol. Cell. Biol. *40*. e00597–e00519. https://doi.org/10.1128/mcb.00597-19.

Wang, M., and Casey, P.J. (2016). Protein prenylation: unique fats make their mark on biology. Nat. Rev. Mol. Cell Biol. *17*, 110–122. https://doi.org/10.1038/nrm.2015.11.

Wensel, T.M., Waldrop, B.A., and Wensel, B. (2010). Pitavastatin: a new HMG-CoA reductase inhibitor. Ann. Pharmacother. *44*, 507–514. https://doi.org/10.1345/aph.1M624.

Widenmaier, S.B., Snyder, N.A., Nguyen, T.B., Arduini, A., Lee, G.Y., Arruda, A.P., Saksi, J., Bartelt, A., and Hotamisligil, G.S. (2017). NRF1 is an er membrane sensor that is central to cholesterol homeostasis. Cell *171*. e15–1101. https://doi.org/10.1016/j.cell.2017.10.003.

Xue, L., Qi, H., Zhang, H., Ding, L., Huang, Q., Zhao, D., Wu, B.J., and Li, X. (2020). Targeting SREBP-2-regulated mevalonate metabolism for cancer therapy. Front. Oncol. *10*, 1510. https://doi.org/10.3389/fonc.2020.01510.

Yamanaka, K., Urano, Y., Takabe, W., Saito, Y., and Noguchi, N. (2014). Induction of apoptosis and necroptosis by 24(S)-hydroxycholesterol is dependent on activity of acyl-CoA:cholesterol acyltransferase 1. Cell Death Dis. *5*, 1–3. https://doi.org/10.1038/cddis.2013.524.

Yang, T., Espenshade, P.J., Wright, M.E., Yabe, D., Gong, Y., Aebersold, R., Goldstein, J.L., and Brown, M.S. (2002a). Crucial step in cholesterol homeostasis: sterols promote binding of SCAP to INSIG-1, a membrane protein that facilitates retention of SREBPs in ER. Cell *110*, 489–500. https://doi.org/10.1016/S0092-8674(02)00872-3.

Yang, T., Espenshade, P.J., Wright, M.E., Yabe, D., Gong, Y., Aebersold, R., Goldstein, J.L., and Brown, M.S. (2002b). Crucial step in cholesterol homeostasis. Cell *110*, 489–500. https://doi.org/10.1016/s0092-8674(02)00872-3.

Yao, X., and Tian, Z. (2015). Dyslipidemia and colorectal cancer risk: a meta-analysis of prospective studies. Cancer Causes Control *26*, 257–268. https://doi.org/10.1007/S10552-014-0507-Y.

Yeh, Y.S., Goto, T., Takahashi, N., Egawa, K., Takahashi, H., Jheng, H.F., Kim, Y. Il, and Kawada, T. (2016). Geranylgeranyl pyrophosphate performs as an endogenous regulator of adipocyte function via suppressing the LXR pathway. Biochem. Biophys. Res. Commun. *478*, 1317–1322. https://doi.org/10.1016/j.bbrc.2016.08.119.

Zeigerer, A., Gilleron, J., Bogorad, R.L., Marsico, G., Nonaka, H., Seifert, S., Epstein-Barash, H., Kuchimanchi, S., Peng, C.G., and Ruda, V.M. (2012). Rab5 is necessary for the biogenesis of the endolysosomal system in vivo. Nature *485*, 465–470. https://doi.org/10.1038/nature11133.

Zhang, Y., Kobayashi, A., Yamamoto, M., and Hayes, J.D. (2009). The Nrf3 transcription factor is a membrane-bound glycoprotein targeted to the endoplasmic reticulum through its N-terminal homology box 1 sequence. J. Biol. Chem. *284*, 3195–3210. https://doi.org/10.1074/jbc.M805337200.

Zinser, E., Paltauf, F., and Daum, G. (1993). Sterol composition of yeast organelle membranes and subcellular distribution of enzymes involved in sterol metabolism. J. Bacteriol. *175*, 2853–2858. https://doi.org/10.1128/JB.175.10.2853-2858.1993.

STAR★METHODS

KEY RESOURCES TABLE

REAGENT or RESOURCE	SOURCE	IDENTIFIER
Antibodies		
Mouse monoclonal anti-Tubulin (clone DM1A)	Sigma-Aldrich	Cat#T9026; RRID: AB_477593
Mouse monoclonal anti-SREBP2 (clone 1C6)	Santa Cruz	Cat#sc-13552; RRID:AB_2194250
Mouse monoclonal anti-c-Myc (clone 9E10)	Santa Cruz	Cat#sc-40; RRID:AB_2857941
Mouse monoclonal anti-HMGCR (clone A9)	MilliporeSigma	Cat#MABS1233
Mouse monoclonal anti-RAB5 (clone D-11)	Santa Cruz	Cat#sc-46692; RRID:AB_628191
Rabbit polyclonal anti-Farnesyl antibodies	Merck Millipore	Cat#AB4073
an unconjugated affinity-purified isotype control immunoglobulin (IgG) from mouse	Santa Cruz	Cat#:sc-2025 RRID: AB_737182
Anti-human NRF3 antibodies (#9408)	Chowdhury et al., 2017	N/A
Chemicals, peptides, and recombinant proteins		
3β-hydroxy-8,24-lanostadiene	Sigma	700063P
Cholesterol-d7	Avanti Polar Lipids	Cat#700041
Nile red	Sigma	72485
RNAiMAX	Invitrogen	Cat# 13778150
ISOGEN II	NIPPON GENE	Cat# 311-07361
SYBR Premix Ex Taq II	Takara Bio	RR820B
Dynabeads Protein G	ThermoFisher Scientific	DB10004
EIPA	Cayman	14406
GGPP	Cayman	63330
FITC-dextran (70 kDa)	TdB Labs	FD70
25-NBD-Cholesterol	Avanti	810250P
NBD-12-Cholesterol	Avanti	810252P
7-AAD	BioLegend	BL420404
VeriBlot for IP Detection Reagent (HRP)	Abcam	ab131366
Critical commercial assays		
PicaGene luciferase assay system	Toyo Ink	PGD-S
LDL uptake assay kit	Abcam	ab236208
NADPH extinction using HMG-CoA Reductase Activity Assay Kit	Abcam	ab204701
Recombinant DNA		
Plasmid: p3×FLAG-CMV 10	Sigma-Aldrich	Cat#E7658
Plasmid: p3×FLAG-CMV 10 harboring the full-length NRF3 genes	Chowdhury et al., 2017	N/A
Plasmid: p3×FLAG-CMV 10 harboring NRF3 lacking NHB1 domain (p3×FLAG-NRF3ΔNHB1)	This paper	N/A
Plasmid: pTK-HSV-BP2 harboring the full-length SREBP2 gene	A gift from Dr. Juro Sakai (The University of Tokyo, Tohoku University); Hua et al., 1996	N/A
Plasmid: pcDNA3.1-6×Myc	Addgene	Cat#128023

(Continued on next page)

Continued

REAGENT or RESOURCE	SOURCE	IDENTIFIER
Plasmid: pcDNA3.1-6×Myc harboring SREBP2 lacking the C-terminal region (p6×Myc-SREBP2ΔC)	This paper	N/A
Plasmid: pCAG-GFP	A gift from Dr. Saturu Takahashi (University of Tsukuba)	N/A
Plasmid: pCAG harboring the full-length mouse Nrf3 tagged with 3×FLAG in the C-terminal region (pCAG-Nrf3-3×FLAG)	This paper	N/A
Experimental models: Organisms/strains		
Mouse: Strain Slc:BDF1	Japan SLC, Inc.	N/A
Mouse: Strain C57BL/6NCrSlc	Japan SLC, Inc.	N/A
Nrf3 transgenic mice generated from Slc:BDF1 injected with the linearized pCAG-Nrf3-3×FLAG plasmid and backcrossed with C57BL/6NCrSlc	This paper	N/A
Experimental models: Cell lines		
Human: HCT116	RIKEN-RCB	RCB2979
Human: H1299	ATCC	N/A
Software and algorithms		
DAVID functional annotation tool	Huang et al., 2009	N/A
GSEA v.3.0	Mootha et al., 2003; Subramanian et al., 2005	N/A
UCSC Genome Browser	Kent et al., 2002	N/A
Deposited data		
Raw and analyzed data	This paper	GEO: GSE176444

RESOURCE AVAILABILITY

Lead contact

Further information and requests for resources and reagents should be directed to and will be fulfilled by the lead contact, Akira Kobayashi (akobayas@mail.doshisha.ac.jp).

Materials availability

All requests for resources and reagents should be directed to and will be fulfilled by the Lead Contact, Akira Kobayashi (akobayas@mail.doshisha.ac.jp). All reagents will be made available on request after completion of a Materials Transfer Agreement.

Data and code availability

The DNA microarray data presented in this study have been deposited in NCBI's Gene Expression Omnibus and are accessible through GEO Series accession number GSE176444.

EXPERIMENTAL MODEL AND SUBJECT DETAILS

Cell lines

HCT116 cells were cultured in DMEM/high glucose medium (Wako Pure Chemical Industries). H1299 cells were also cultured in an RPMI-1640 medium (NacalaiTesque). All media were supplemented with 10% FBS (Nichirei Biosciences), 40 μg/mL streptomycin, and 40 units/mL penicillin (Life Technologies). Our laboratory previously generated GFP and NRF3 overexpression H1299 cells (Waku et al., 2020b).

Generation of Nrf3-Tg mouse

A DNA fragment encoding the full-length mouse Nrf3 tagged with 3×FLAG in the C-terminal region was inserted into the EcoRI site of the pCAG-GFP plasmid (pCAG-Nrf3-3×FLAG). After the standard transgenic mouse procedure, the linearized plasmid was injected into BDF1 × BDF1 fertilized eggs (Ainoya et al., 2012). Transgene-positive founder mice were identified by PCR using the following primers; forward (5′-TGAGGCAGAAGCTACATGGC-3′) and reverse (5′-GTCACTGGAGCTATTCAGTTTC-3′). Additionally, Nrf3-Tg mice obtained were backcrossed with C57BL/6J mice, and mice of first and third generations of the backcross were analyzed. The efficiency of overexpression in colorectal tissues is summarized in Figures S1E and S1F. Mice were housed in a specific pathogen-free facility, and the experimental protocol was approved and executed under the Ethics Review Committees for Animal Experiments of Doshisha University and Tohoku University.

METHOD DETAILS

Transfection

Transfection of plasmid DNA and siRNA was performed using polyethyleneimine and RNAiMAX (Invitrogen), respectively. The sequences of the siRNA duplexes are listed in Table S6. The efficiency of overexpression or knockdown in cells is summarized in Figures S1A–S1D.

RNA extraction and RT-qPCR

Total RNA was extracted and purified using ISOGEN II (NIPPON GENE) according to the manufacturer's instructions. Aliquots of total RNA (1 μg) were reverse transcribed using pd (N)6 random primer (Takara Bio) and Moloney murine leukemia virus reverse transcriptase (Invitrogen) with a 250-μM deoxy nucleoside triphosphate (Takara Bio) concentration, according to the manufacturer's instructions. RT-qPCR was also performed using SYBR Premix Ex Taq II (Takara Bio), and primers for genes were conducted using a Thermal Cycler Dice Real-Time System (Takara Bio). Each gene expression level in human cells was also normalized to the mRNA levels of the human β-actin gene. qPCR primer sequences are described in Table S6.

DNA microarray analysis

DNA microarray data of H1299-oeNRF3 and p53KO HCT116-siNRF3 cells were obtained as described in our previous study in which the DNA microarray of HCT116-siNRF3 cells was reported (Waku et al., 2020a). Briefly, total RNA was processed with the Ambion WT Expression Kit (Affymetrix) according to the manufacturer's instructions. cRNA was then fragmented, labeled, and hybridized to the Affymetrix Human Gene 1.0 ST Arrays using the GeneChip WT Terminal Labeling and Hybridization Kit (Affymetrix). GeneChip fluidics station 450 was used for processing the arrays, and fluorescent signals were detected using the GeneChip scanner 3000–7 G. The expression console and transcription analysis console (Affymetrix) were used to analyze the data.

The DAVID functional annotation tool was also used for GO analysis of the biological process of the 100 common genes in H1299-oeNRF3, HCT116-siNRF3, and p53KO HCT116-siNRF3 cells (see the Results section for details) (Huang et al., 2009). The expression data of all genes in these DNA microarrays were subjected to a GSEA using open-source software v.3.0 (Mootha et al., 2003; Subramanian et al., 2005). The gene set related to fatty acid metabolism (HALLMARK_FATTY_ACID_METABOLISM) was downloaded from the Molecular Signatures Database v7.2 as well.

Immunoblot analysis

To prepare whole-cell extracts, the cells were lysed with an SDS sample buffer (50 mM Tris–HCl [pH 6.8], 10% glycerol, and 1% SDS). The protein quantities in the cell extracts were measured using a BCA kit (Wako Pure Chemical Industries). The proteins were then separated using SDS-PAGE and transferred to PVDF membranes (Immobilon-P transfer membrane, EMD Millipore Corporation). After blocking the membranes with a Blocking One (NacalaiTesque) at 4°C overnight, the membranes were incubated with a primary antibody, washed with TBS-T (20 mM Tris–HCl [pH 7.6], 137 mM NaCl, and 0.1% Tween20) and were incubated with a horseradish peroxidase-conjugated secondary antibody (Invitrogen). The blots were then washed with TBS-T and developed with enhanced chemiluminescence (GE Healthcare). All immunoblot analyses in this study were performed in two independent experiments.

Co-IP experiments

PCR amplification was used to generate a DNA fragment encoding the NRF3 lacking NHB1 domain (NRF3ΔNHB1). It was also used to generate the SREBP2 lacking the C-terminal region (SREBP2ΔC) of the p3×FLAG-CMV 10 harboring the full-length NRF3 genes (Chowdhury et al., 2017) or the pTK-HSV-BP2 plasmid harboring the full-length *SREBP2* gene (Hua et al., 1996). A Prime STAR GXL premix (TaKaRa) with the primers described in Table S6 was used. Then, each fragment was inserted into the KpnI and BamHI sites of the p3×FLAG-CMV 10 vector (p3×FLAG-NRF3ΔNHB1) or the Xho1 and Xbal1 sites of the pcDNA3.1-6×Myc vector (p6×Myc-SREBP2ΔC), respectively. Sequencing confirmed all constructs.

HCT116 cells were co-transfected with p3×FLAG-NRF3ΔNHB1 and p6×Myc-SREBP2 ΔC vectors. At 24 h after co-transfection, the cells were lysed using the NETN Buffer (20 mM Tris–HCl [pH 8.0], 100 mM NaCl, 1 mM EDTA, 0.1% NP-40, and 1 mM DTT) in the presence of protease inhibitors (NacalaiTesque). After rotating with anti-IgG (Santa Cruz) or anti-Myc (Santa Cruz) antibodies for 5 h at 4°C, Protein G Sepharose beads were added and rotated again for 24 h at 4°C. The beads were then washed with the NETN buffer three times and then subjected to immunoblot analysis.

Co-IP experiments for RAB5 prenylation were performed as described previously (Bertolio et al., 2019). Briefly, H1299-oeNRF3 or oeGFP was lysed using the IP buffer (20-mM Tris–HCl [pH 8.0], 120-mM NaCl, 1-mM EDTA, 0.5% NP-40) in the presence of protease inhibitors (NacalaiTesque). After pre-cleaning with Dynabeads Protein G (ThermoFisher Scientific) for 1 h at 4°C, the lysate was rotated with anti-IgG (Santa Cruz) or anti-RAB5 (Santa Cruz) antibodies bound to Dynabeads Protein G for 3 h at 4°C. The beads were then washed with the IP buffer three times and then subjected to immunoblotting using anti-RAB5 (Santa Cruz) or anti-Farnesyl antibodies (Merck Millipore) with VeriBlot for IP Detection Reagent (HRP) (abcam, ab131366), according to the manufacturer's protocol.

Co-IP experiments in this study were performed in two independent experiments.

ChIP-qPCR

The cells were treated with 1 μM MG-132, a proteasome inhibitor (Peptide Institute). After 24 h, the cells were fixed with 1% formaldehyde for 10 min at room temperature, and then, glycine was added to make a final concentration of 0.125 M. The cells were then lysed using a cell lysis buffer (5 mM Tris–HCl [pH 8.0], 85 mM KCl, and 0.5% NP-40) with protease inhibitors (NacalaiTesque) and then centrifuged at 2,000 rpm at 4°C for 3 min. The pellets were further lysed using a nuclei lysis buffer (50 mM Tris–HCl [pH 8.0], 10 mM EDTA, and 1% SDS) with protease inhibitors (NacalaiTesque), after which the lysates were sonicated. After centrifugation at 15,000 rpm at 8°C for 10 min, the supernatants were collected. The supernatants were then diluted in a ChIP dilution buffer (16.7 mM Tris–HCl [pH 8.0], 167 mM NaCl, 1.2 mM EDTA, 1.1% TritonX-100, and 0.01% SDS). Also, the diluted samples were pre-cleared with 20 μL of Dynabeads Protein G (ThermoFisher Scientific); then, the supernatants (used as an input sample) were incubated with 2 μg of anti-NRF3 antibody. The immunocomplexes were also collected by incubation with 20 μL of Dynabeads Protein G (ThermoFisher Scientific) and then washed with the following buffers: the low salt wash buffer (20 mM Tris–HCl [pH 8.0], 150 mM NaCl, 2 mM EDTA, 1% Triton X-100, and 0.1% SDS), high salt wash buffer (20 mM Tris–HCl [pH 8.0], 500 mM NaCl, 2 mM EDTA, 1% Triton X-100, and 0.1% SDS), and LiCl wash buffer (10 mM Tris–HCl [pH 8.0], 250 mM LiCl, 1 mM EDTA, 1% sodium deoxycholate, and 1% NP-40). Finally, the beads were washed twice with 1 mL of TE buffer (10 mM Tris–HCl [pH 8.0], and 1 mM EDTA). The immunocomplexes were then eluted by adding 200 μL of elution buffer (50 mM $NaHCO_3$ and 1% SDS). After reverse cross-linking by adding 200 mM NaCl, the remaining proteins were digested by adding proteinase K. For quantification of NRF3 binding to the target regions, RT-qPCR was then performed using the purified DNA with the primers described in Table S6.

Luciferase reporter assays

PCR amplification generated the luciferase reporter driven by the *HMGCR* promoter of the human genomic DNA. This analysis was conducted using a Prime STAR HS DNA polymerase (TaKaRa) with the following primers; forward (5′-TTTGAGCTCTGGGTAAATCTCGGGAAAGC-3′) and reverse (5′-TTTCTCGAGGAAGGAGCCCT CACCTTACG-3′), and cloned into the pGL3-Control Vector (Promega). Sequencing confirmed the construct.

Cells expressing the reporters indicated in the legend for Figure 3D were then lysed. Luciferase activities were also measured using a microplate reader (Synergy HTX, Bio Tek Instruments) and PicaGene luciferase assay system (Toyo Ink) according to the manufacturer's instructions.

GC-MS

To measure the levels of lanosterol and cholesterol, GC-MS analysis was performed as described previously (Yamanaka et al., 2014). The cells in the 1.1 mL PBS solution were then divided into 100-μL solutions for BCA assay and 1 mL for lipid extraction. For lipid extraction, 50-μL methanol containing internal standards, 3β-hydroxy-8,24-lanostadiene (Sigma) and Cholesterol-d7 (Avanti Polar Lipids) were added. The solutions were then mixed with 1 M KOH in methanol (1 mL). After incubation for 30 min at 40°C, 2 mL chloroform and 1 mL water were added and mixed using a vortex mixer for 1 min and centrifuged at 3,500 ×*g* for 10 min at 4°C. The chloroform layer was also extracted and evaporated to dryness under nitrogen for gas chromatography. As a silylating agent, TMSI-H (GL Sciences) was added to the dried residue. An aliquot of this sample was then injected into a gas chromatograph (QP2010 Ultra/SE SHIMADZU). Helium was used as the carrier gas at a flow rate of 43 cm/s. Temperature programming was also conducted to control the temperature from 50°C to 250°C at 30°C/min and 250°C–325°C at 5°C/min. The injector temperature was also set to 280°C, and the temperature of the ion source was set to 200°C. Lanosterol and cholesterol were identified on the basis of their retention times and mass patterns.

Nile red staining

The cells were stained with 10 μM Nile red (Sigma) for 5 h, after which they were washed twice with FACS buffer (0.1% [w/v] sodium azide and 2% FBS in cold PBS). The samples are then subjected to flow cytometry (FACSAriaII, BD Biosciences).

LDL uptake assay

LDL uptake assays were conducted using the LDL uptake assay kit (Abcam) according to the manufacturer's protocol. Cells were seeded onto 6-well plates. After 24 h, the cells were labeled with 1 μM LDL-DyLight 488 for 4 h and then resuspended in a 7-AAD staining buffer. The sample was then subjected to LDL uptake assay using a flow cytometer (FACSAriaII, BD Biosciences).

Macropinocytosis assay

Macropinosome was stained as described previously (Commisso et al., 2014). Briefly, the cells were incubated in serum-free medium for 10 h and then pretreated with 100 μM EIPA (Cayman) or DMSO for 1 h. Then, either 1 mg/mL FITC-dextran (70 kDa, TdB Labs), 1 mg/mL FITC-BSA (Invitrogen), 1 μM 25-NBD-Cholesterol (Avanti), 1 μM NBD-12-Cholesterol (Avanti), or 1 μM (LDL-DyLight 488) was added to the serum-free medium for 1 h. The cells were also fixed in 3.7% (v/v) formaldehyde/PBS for 30 min, followed by washing twice with an FACS buffer (0.1% [w/v] sodium azide and 2% FBS in cold PBS). Then, the cells were resuspended in 500 μL FACS buffer containing 1 μg/mL 7-AAD (BioLegend). After treatment for 10 min in the dark, the sample was subjected to flow cytometry (FACSAriaII, BD Biosciences).

HMGCR activity assay

The enzymatic activity of HMGCR was evaluated by quantifying the NADPH extinction using HMG-CoA Reductase Activity Assay Kit (abcam, ab204701). The assay was performed as described previously (Li et al., 2019). Briefly, the cells were lysated by the cell lysis buffer (20-mM Tris [pH 7.5], 150-mM NaCl, and 1% Triton X-100). Then, cell lysates were loaded on a 96-well plate, and enzyme reagent was added to each well in the following order: 1 × assay buffer, reconstituted NADPH, and substrate solution (HMG-CoA). Finally, the samples were mixed thoroughly. The optical absorbance of each well was measured at 340 nm. HMGCR inhibitor atorvastatin was used as a negative control, and lysis buffer was used as blank.

QUANTIFICATION AND STATISTICAL ANALYSIS

Data are reported as mean ± standard deviation (SD). Mann–Whitney *U*-test or Welch's *t*-test was used to compare the two groups with equal or unequal sample sizes, respectively. One-way analysis of variance followed by Tukey's post hoc test was used to compare multiple groups.